Ab Initio Study of the Interaction of Water with Cluster Models of the Aluminum Terminated (0001) α-Aluminum Oxide Surface

J. M. Wittbrodt, W. L. Hase,* and H. B. Schlegel*

Department of Chemistry, Wayne State University, Detroit, Michigan 48202

Received: March 17, 1998; In Final Form: June 3, 1998

Ab initio calculations were performed on three cluster models to investigate the interaction of water with the (0001) surface of α-Al_2O_3. Surface relaxation effects are found to be similar to those in previous periodic Hartree−Fock and density functional calculations. Two types of dissociative reactions, 1−2 and 1−4 addition of water, were explored. Catalysis of the 1−4 addition reaction by a second water molecule was also examined. Of these three routes to hydroxylation of the aluminum terminated surface, the two water process was found to be the most exothermic. In all cases, little difference is observed between the energies of molecular and dissociative adsorption of one water. Multiple 1−2 dissociation events at a single surface site were also explored and found to be overall exothermic. Transition state theory was used to calculate molecular → dissociative adsorption unimolecular rate constants. Both the 1−2 and 1−4 dissociations are predicted to be rapid processes at 300 K, occurring within 10^{-2} s.

I. Introduction

As one of the most important ceramic materials, α-aluminum oxide has been the subject of numerous experimental[1−5] and theoretical studies.[6−12] It is used extensively as a substrate for thin films and as a catalyst support. It can also serve as a model for oxide surfaces on aluminum metal. Adhesive bonds between aluminum oxide surfaces and polymers are widely used in the construction of lightweight materials and devices.[13,14]

Of the various cleavage planes, the aluminum terminated (0001) face of α-Al_2O_3 has been predicted by various theoretical methods to be the most stable.[7−9] Figure 1 shows six atomic layers (two Al−O−Al stacking sequences) of this surface. Seen from above, the hexagonal unit cell is a rhombus, eighteen atomic layers deep. Twelve of these layers consist of a single aluminum atom; the remaining layers each contain three oxygen atoms which form an equilateral triangle. Each surface aluminum has below it three nearest neighbor oxygen atoms, each of which has two additional, inequivalent neighboring aluminum atoms at distances of 1.857 and 1.969 Å. In the second aluminum layer, each atom has three oxygen atoms above at the short Al−O distance and three below at the long Al−O distance. In the third layer of aluminum atoms, which begins the next Al−O−Al stacking unit, the short/long pattern is reversed. Two other (0001) surfaces are also possible. Cleavage of the crystal along the plane indicated by cut 1 in Figure 1b yields the oxygen terminated surface, while along cut 2, a double aluminum layer surface, is produced. Cleavage between two aluminum layers, as in cut 3, reproduces the single layer termination of Figure 1a.

A key theoretical result for this aluminum terminated surface is a large relaxation of the top layer of aluminum atoms, with the distance to the oxygen plane decreasing by 48−86%, accompanied by smaller changes in the spacings of the next few atomic layers.[9−11] This has recently been observed experimentally both by Guenard et al.,[4] who conclude from grazing incidence X-ray scattering that the first interplanar spacing decreases by 51%, and by Ahn and Rabalais,[5] whose

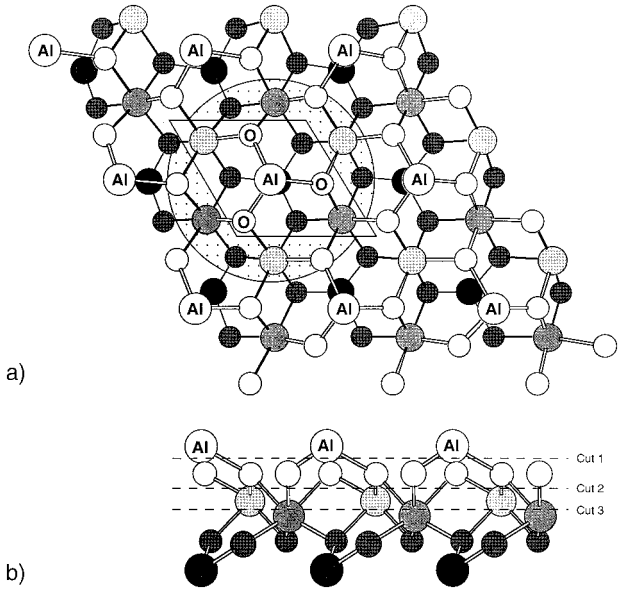

Figure 1. Aluminum terminated (0001) α-Al_2O_3 surface. Top (a) and front (b) views of six atomic layers are shown. The rhombus in part a encloses a unit cell. The circled, shaded portion is the Al_8O_{12} cluster model used in this study. In part b, cut 1 exposes the oxygen terminated surface; cut 2, a double-layer aluminum surface; and cut 3, the same surface shown in this figure.

time-of-flight scattering and recoiling spectrometry study indicates a 63% relaxation. Although aluminum terminated surfaces may exist under vacuum,[1,3] it is likely that surfaces exposed to oxygen and water have different terminations. High-resolution electron-energy-loss spectroscopy (HREELS) experiments by Coustet and Jupille[2] indicate that OH groups on the hydroxylated (0001) surface occupy positions consistent with a perfect oxygen terminated surface. In a recent theoretical study, Nygren et al.[12] conclude that the oxygen terminated surface is stabilized by hydroxylation and that relaxation of the resulting surface occurs to a lesser extent than for the clean aluminum terminated surface. It was also noted that since the atoms in the oxygen terminated

S1089-5647(98)01516-8 CCC: $15.00
Published on Web 08/05/1998

surface are associated with two aluminum layers, exposure to water of the single-layer aluminum termination may not lead to the same hydroxylated surface. Formation of such a surface would require either surface reconstruction or removal of the surface aluminum.

Aluminum oxide surfaces arising in industrial manufacturing are usually amorphous and hydroxylated. A variety of contaminants, including water and oils, may be adsorbed on these surfaces.[15,16] Often an adhesive is applied directly to this contaminated surface. Thus, the strength and durability of the adhesive/aluminum oxide bond depends on a number of different chemical and physical interactions. Clearly, understanding the energetics and resulting structure(s) for water association with aluminum oxide surfaces is an important first step in characterizing the adhesion of polymer materials to hydroxylated aluminum oxide surfaces.

In this paper we report the results of a series of ab initio calculations used to study the interactions of one or more water molecules with cluster models of aluminum oxide surfaces. Figure 2 shows three models of a Lewis acid site on the aluminum terminated surface of Figure 1a. Model 1, AlF_3, is a simple model of the tricoordinate aluminum site, with the highly electronegative fluorines mimicking the ionicity of the oxide. This model was used primarily to determine an appropriate level of theory for use on the larger models by examining the binding energy of AlF_3-H_2O. Model 2, an Al_4O_6 adamantane-like structure, was chosen because of its correct stoichiometry, tricoordinate aluminum sites, and relatively simple geometry. This model was used to investigate molecular and 1−2 dissociative adsorption of water. The final model of the (0001) surface, model 3, is a twenty atom Al_8O_{12} cluster of S_6 symmetry clipped from the bulk structure of α-Al_2O_3.[17,18] This cluster may be seen in the context of the entire surface by referring to the circled and shaded portion of Figure 1a.

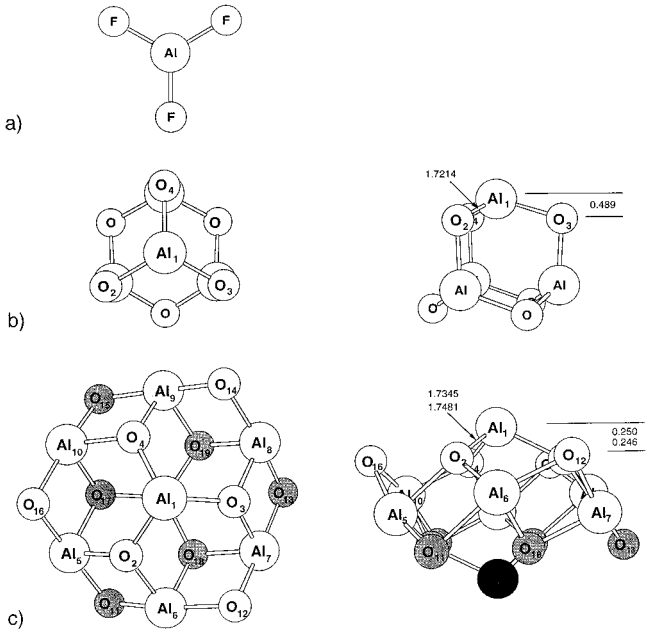

Figure 2. Cluster models of the aluminum surface site: (a) model 1, AlF_3; (b) top and front views of model 2, Al_4O_6; (c) top and front views of model 3, Al_8O_{12}, taken from an ideal termination of the bulk crystal (see Figure 1a). Distances are in angstroms and are optimized as described in the text at the HF and (lower set of numbers) B3LYP levels of theory.

II. Computational Details

Ab initio calculations for the three cluster models discussed above were performed with the GAUSSIAN 94[19] series of programs. For model 1, geometries and energies of AlF_3, H_2O, and their complex, AlF_3-H_2O, were obtained using B3LYP hybrid density functional theory (DFT)[20] with both the 6-31G* and 6-31+G* basis sets. Energies were also computed with the high-accuracy G2(MP2)[21] and CBS-Q[22] methods. Results were compared to the Hartree−Fock calculations of Scholz et al.[23] and the MP2 calculation of Ball.[24] The structures studied for model 2 include Al_4O_6, molecular and dissociative adsorption of water on Al_4O_6, and the transition state for dissociation. Geometries for these structures were fully optimized and the harmonic vibrational frequencies computed at the HF/6-31+G* level of theory. B3LYP/6-311+G* and MP2/6-311+G* energies were also computed at these geometries. For model 3, two sets of calculations were performed. The first set contains four structures analogous to those of model 2; an Al_8O_{12} cluster with surface atoms relaxed (model 3a), molecular adsorption of water on Al_8O_{12}, and the product and transition state for 1−2 dissociative adsorption across the Al_1-O_2 bond of Al_8O_{12} (see Figure 2c). Also included are two clusters modeling products of multiple 1−2 dissociative adsorptions. The second set of calculations for model 3 was motivated by Car−Parrinello calculations performed by Hass et al.,[25] which indicate that addition of water can also occur via 1−4 processes, in which a hydrogen adds not to an oxygen adjacent to the surface aluminum but to a second nearest oxygen (atom 16 in Figure 2c). They also found that 1−4 addition of water could be catalyzed by a second water molecule. Modeling these reactions are the following: a relaxed Al_8O_{12} cluster (model 3b), molecular and dissociative adsorption minima for both the one and two water processes, and the transition states for dissociative adsorption.

To retain the general structure of the bulk crystal, the positions of some of the atoms in model 3 were constrained. Coordinates of selected surface atoms were optimized for all structures at the Hartree−Fock level of theory and, in some cases, at the B3LYP level of theory as well. For model 3a, the optimized atoms are those of the surface AlO_3 group (atoms 1−4 in Figure 2c) and the adsorbing water molecule(s). In model 3b, which considers 1−4 dissociative adsorption of water, the coordinates of O_{16} are also optimized. However, because this atom is on the edge of the cluster and is missing one-third of its coordinating aluminum atoms, the dihedral angle (16, 17, 10, 5) was frozen at the bulk value of zero to prevent an unrealistically large relaxation into the empty space that would otherwise be occupied by the bulk crystal. All nonoptimized atoms were frozen at their bulk Cartesian coordinates as obtained from Cerius^2.[17]

Because the cost of these ab initio calculations increases approximately as the cube of the number of basis functions, we chose to represent the atoms to be optimized (e.g. atoms 1−4 in model 3a) with the 6-31+G* basis set and the remaining atoms with the smaller 3-21G basis set. For model 3b, Al_5 and Al_{10}, as well as atoms 1−4 and O_{16}, are represented by the larger 6-31+G* basis set since they connect the additional optimized oxygen to the AlO_3 center. The basis sets for these types of calculations are denoted as 6-31+G*(3-21G). For some structures, energies were also computed at the HF/6-31+G* and/or B3LYP/6-31+G* levels of theory on geometries optimized using the smaller 6-31+G*(3-21G) basis set.

As a preliminary assessment of the contribution of long-range Coulombic effects present in the ionic crystal, several of the previously optimized clusters were embedded in a field of approximately 2000 point charges placed in bulk atom positions.

TABLE 1: Relaxation Energy of Model 3A, Al_8O_{12}

level of theory	relaxation energy[a] (kcal/mol)	level of theory	relaxation energy[a] (kcal/mol)
HF/6-31+G* (3-21G)	52.06	B3LYP/6-31+G*(3-21G)	37.70
HF/6-31+G*//HF/6-31+G*(3-21G)	53.36	B3LYP/6-31+G*//B3LYP/6-31+G*(3-21G)	40.95
B3LYP/6-31+G*//HF/6-31+G*(3-21G)	38.50		

[a] Decrease in the potential energy when the structure of Al_8O_{12} is optimized from the bulk geometry with the constraints given in the text.

A cutoff function with a range of ca. 20 Å was applied to achieve approximately the same Madelung potential at the central surface aluminum as given by the full surface ($\exp[-(2.05 \times 10^{-7})\, d^6]$, d = distance (Å) to the central surface aluminum atom). Two sets of charges were used. First, formal charges of +3 and −2 were place at the lattice positions. (This should provide an upper bound to the Coulombic effects.) Single point energies were computed at the HF/6-31+G*(3-21G) level of theory, and selected surface atoms of the clusters were then further relaxed in the field of formal point charges. Second, an improved, more realistic electrostatic environment was constructed by using the average HF/6-31+G*//HF/6-31+G*(3-21G) charges from the unembedded cluster (+2.31 and −1.54), placing them at the lattice positions with the z coordinate of the surface Al atoms relaxed by the amount obtained for the unembedded cluster (0.584 Å), and applying the above cutoff function. Although leakage of electron density from edge anions is a common concern for clusters embedded in an array of point charges, it is expected that the use of the small 3-21G basis set on the edge atoms will help prevent this. Since model 3b contains an edge oxygen with the larger basis set, embedding was done only for model 3a clusters.

Harmonic frequencies at the HF/6-31+G*(3-21G) level of theory were computed for a number of model 3 structures. Any atom which had been frozen during the geometry optimization was frozen in the frequency calculation as well. The surface O−H frequencies are of primary interest, particularly since the remaining $(Al_2O_3)_n$ cluster modes cannot be expected to model the lattice modes of an infinite surface. The frequencies computed for models 2 and 3 were scaled by 0.8973, which is the scaling factor determined by Knosser et al.,[26] to give the best agreement between the experimental anharmonic and the HF/6-31+G* frequencies for H_2O.

III. Results and Discussion

A. Cluster Models and the α-Aluminum Oxide Surface. The structures and electrostatics of the cluster models were analyzed for comparison with the aluminum terminated α-aluminum oxide surface.

1. Surface Relaxation. Optimized geometries for Al_4O_6 and Al_8O_{12} (model 3a) are shown in Figure 2. In these latter calculations, only the positions of the four AlO_3 surface atoms are optimized and the resulting surface relaxation examined. During relaxation from the bulk geometry (see Introduction), each Al_{surf}−O distance decreases by 0.12 Å at the HF/6-31+G*-(3-21G) level of theory, while the B3LYP/6-31+G*(3-21G) change is slightly smaller; i.e., 0.10 Å. In general the short O−Al distances, between the surface O atoms and the second layer of Al atoms, become somewhat shorter, while the long O−Al distances, between these O atoms and the third layer of Al atoms, become slightly longer. For Hartree−Fock, these changes result from a 0.584 Å downward relaxation of the surface aluminum atom and a 0.004 Å upward motion of the three neighboring oxygen atoms. At the B3LYP level of theory, the relaxation of the surface aluminum is ca. 0.04 Å smaller, while the upward displacement of the three oxygen atoms is 0.04 Å larger. Thus, the $Al_{surf}-3O_{plane}$ separation decreases by approximately 70% to 0.25 Å at both levels of theory. The spacing between the 3O plane and the second layer of Al atoms increases by less than 1% for the HF calculation and by 5.7% for the B3LYP calculation. The structural changes that occur during relaxation for this cluster model are comparable to changes that occur in extended models of the (0001) surface. Periodic DFT calculations done in the local density approximation (LDA) by Manassidis et al.[10] predict an 86% decrease in the spacing between the Al_{first} and O_{first} planes and a 3% increase between the O_{first} and Al_{second} planes. Periodic HF calculations by Puchin et al.[11] give a 68% decrease in the $Al_{first}-O_{first}$ spacing and a 0.6% decrease in the $O_{first}-Al_{second}$ spacing. The relaxed Al−3O interplanar spacing of 0.25 Å also compares well to the experimental result of Ahn and Rabalais,[5] of 0.3 ± 0.1 Å.

TABLE 2: Al and O Charges for the Cluster Models[a]

			Al_8O_{12}, model 3a[c]	
	AlF_3[b]	Al_4O_6[b]	surface	bulk average
Al	2.38	2.27	2.30, 1.97, 1.91	1.9, 2.4, 2.4
O		−1.51	−1.62, −1.67, −1.66	−1.2, −1.5, −1.5

[a] Determined by a natural population analysis [29] [b] HF/6-31+G* level of theory. [c] HF/6-31+G*(3-21G) level of theory. Refer to section A2 of the discussion for the definition of surface and bulk atoms and description of the three reported charges.

Relaxation energies determined from these model 3a calculations range from 38 to 53 kcal/mol (Table 1). Values computed with the B3LYP method are 11−14 kcal/mol smaller than the HF results. When converted to units of J/m^2 (using a surface area of 19.55 Å^2),[27] the values of the relaxation energy range from 1.34 to 1.90 J/ m^2. This compares well to 1.21 J/ m^2, obtained by the periodic HF calculations of Causà et al.,[9] and to 2.01 J/ m^2, the DFT (LDA) result of Manassidis et al.[10,28]

The geometry changes that occur during relaxation of Al_8O_{12} model 3b, where O_{16} is partially optimized, are slightly more complicated than those of model 3a. Most Al−O are within 0.02 Å of their previously optimized values. However the $O_{16}-Al_5$ long distance is approximately 0.2 Å shorter than the other Al−O long distances, due to a downward relaxation of O_{16} which is attributed to the lack of a surface aluminum atom in the neighboring cell. With the additional optimized oxygen, relaxation energies are 5−8 kcal/mol larger than the results for model 3a, where only the AlO_3 group is optimized.

2. Electrostatics. The atomic charges of Al and O for the optimized cluster models are listed in Table 2. The charges were determined by natural population analysis[29] and are similar for the different models. Three sets of charges, for both surface and bulk atoms, are reported for model 3a, Al_8O_{12}. The surface atoms are those of the optimized AlO_3 surface group. The remaining atoms comprise the "bulk" for which average Al and O charges are given. The first set of charges is for the optimized Al_8O_{12} geometry, the second for this optimized geometry embedded in the "sea" of formal point charges of +3 and −2, and the third for the geometry reoptimized in these formal point charges. For the unembedded relaxed cluster, the AlO_3 site has charges of +2.30 and −1.62, while the average "bulk" Al and O atoms, represented by the smaller basis set, have charges of

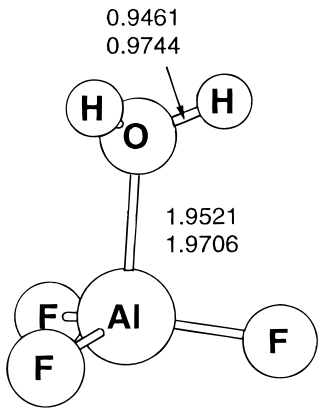

Figure 3. Adsorption of water to model 1, AlF_3, at the HF/6-31+G* and (lower set of numbers) B3LYP/6-31+G* levels of theory. Bond lengths are in angstroms.

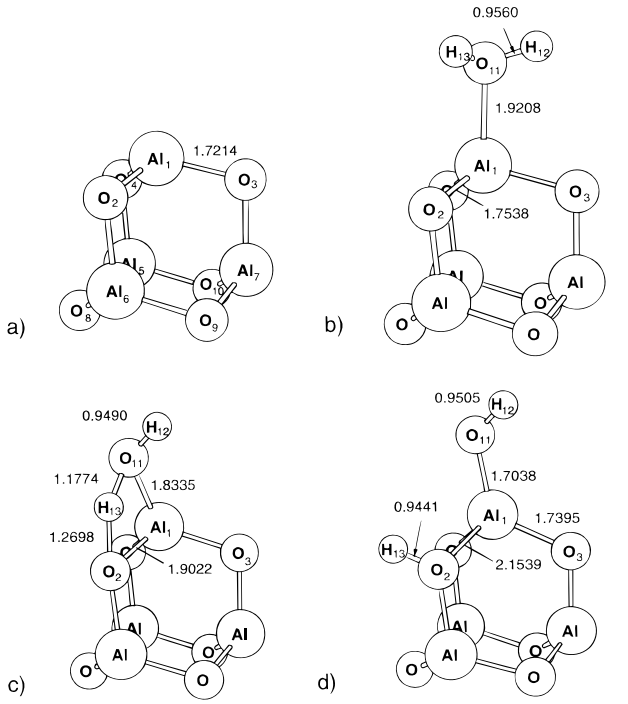

Figure 4. Adsorption of water on model 2 at the HF/6-31+G* level of theory. The structures are as follows: (a) the Al_4O_6 cluster model, (b) molecular adsorption, (c) transition state, and (d) dissociative adsorption.

+1.9 and −1.2. Adding the field of formal point charges, without reoptimization of the geometry, decreases the surface Al charge to +1.97 while increasing the O_{surf} charge to −1.67. The ionicity of the bulk is also increased, giving charges of +2.4 and −1.5 that are comparable to +2.75 and −1.83 predicted by Ching and Xu.[30] Reoptimization in the field of formal charges leads to an even smaller Al_{surf} charge of +1.91, while the O_{surf} charge changes only slightly to −1.66 and the bulk charges do not change significantly.

B. Molecular Physisorption. Structures for molecular adsorption of water on the different cluster models are shown in Figures 3, 4b, and 5b. In the AlF_3-H_2O complex the Al−O distance is 0.9% longer at the B3LYP/6-31+G* level of theory than for the same basis set Hartree−Fock result. Binding energies computed at various levels of theory for this complex are summarized in Table 3. Values calculated without diffuse functions are 2−6 kcal/mol larger than the G2(MP2) and CBS-Q results. When corrected for basis set superposition error ($\Delta E_{BSSE} = -2.4$ kcal/mol), the MP2/6-31G** value[24] is within 1 kcal/mol of the results of the high-accuracy energy methods, while the (uncorrected) values for the HF and B3LYP calculations which include diffuse functions are within 2 kcal/mol. This indicates that HF/6-31+G* and B3LYP/6-31+G* are both reasonable levels of theory for exploring $(Al_2O_3)_n-H_2O$ interactions in the larger systems of model 2 and model 3.

The optimized structure for molecular adsorption of water on model 2 at the HF/6-31+G* level of theory is shown in Figure 4. The H_2O-Al distance of 1.921 Å is similar to that of model 1 and is about 0.2 Å longer than the Al−O distances in the cluster. During adsorption, the $Al_{surf}-O$ distances in the cluster lengthen by less than 0.03 Å (2%), while the distance between the surface aluminum and the first oxygen plane increase by 17% (0.084 Å). The molecular adsorption energies, summarized in Table 4, are in the range 39−45 kcal/mol and are 10 kcal/mol greater than for model 1.

Figure 5b shows the structure for molecular adsorption on the model 3a Al_8O_{12} cluster. The HF H_2O-Al distance of 1.93 Å is similar to those of models 1 and 2. Molecular adsorption of water increases the Al−3O spacing by 0.14 Å, reversing approximately 25% of the downward displacement that occurred for Al_{surf} during relaxation. Molecular adsorption energies (Table 5) computed with the 6-31+G*(3-21G) basis set, for both the HF and B3LYP methods, fall within the range of values predicted by model 2.

Molecular adsorption was also studied at the HF/6-31+G*-(3-21G) level of theory for model 3a embedded in a field of formal point charges. Simply adding the field to the relaxed Al_8O_{12} cluster without reoptimizing the geometry destabilizes molecular adsorption by 17 kcal/mol. Optimization in the field of formal point charges lowers the molecular adsorption energy, putting it only 5 kcal/mol above the value obtained without point charges. The cluster was also embedded in the improved field that takes into account the average charges and relaxation of surface aluminums in the lattice. In this environment, single point calculations on the Al_8O_{12} cluster (previously optimized in the absence of point charges) give a molecular adsorption energy of 44 kcal/mol, and calculations using an $Al_{18}O_{27}$ cluster yield 48 kcal/mol.[31] These energies are very similar to the MP2 results without point charges in Table 4.

Although molecular adsorption of a single water molecule was also examined as part of the calculations for model 3b, the field of point charges was not considered because the active site now extends to the edge of the cluster and loss of electron density from O_{16} could be a problem. However, the results for the unembedded model 3b clusters are essentially the same as for model 3a.

C. 1−2 Dissociative Adsorption. The molecularly adsorbed water can undergo a 1−2 dissociative chemisorption step. This process was studied with the model 2 and model 3a calculations. The resulting transition state and chemisorbed product structures are given in Figures 4 and 5; the energetics appear in Tables 4 and 5. In proceeding from molecular to dissociative adsorption for model 2, the $Al_{surf}-O$ across which dissociation occurs lengthens by 0.400 Å. Meanwhile, the $Al_{surf}-O_{ads}$ distance decreases to 1.704 Å, comparable to the other "normal" Al−O contacts. A large portion of the changes in the Al−O interactions are caused by the adsorbing water pulling upward on the surface aluminum atom. The distance of the surface aluminum to the first oxygen plane is increased during dissociative adsorption by 0.341 Å. The transition state is roughly 35% of the way between molecular and dissociative adsorption, as judged by the changes in the O−H and Al−O distances.

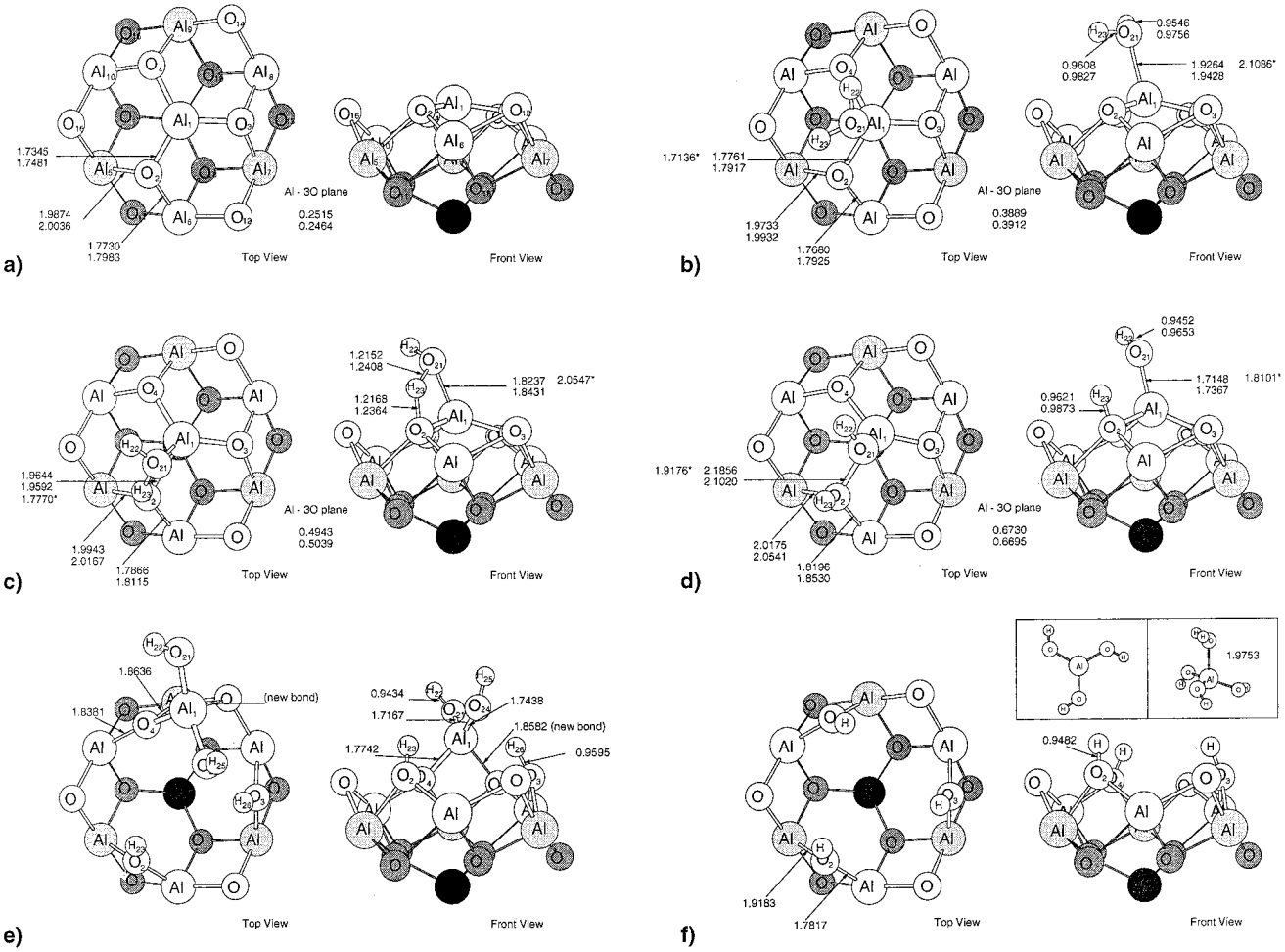

Figure 5. Model 3, set 1 at the HF/6-31+G*(3-21G) and (lower set of numbers) B3LYP/6-31+G*(3-21G) levels of theory. Distances for the optimizations in the field of point charges are marked with an asterisk. Structures are as follows: (a) the Al_8O_{12} relaxed cluster, (b) molecular adsorption, (c) dissociative adsorption transition state, (d) dissociative adsorption, (e) dissociative adsorption of two water molecules, and (f) dissociative adsorption of three water molecules, resulting in removal of the surface aluminum atom to form $Al(OH)_3$. This product is also shown with an additional adsorbed water as $Al(OH)_3 \cdot H_2O$.

TABLE 3: Binding Energy of $AlF_3 \cdot H_2O$

level of theory	binding energy (kcal/mol)	level of theory	binding energy (kcal/mol)
HF/6-31G*	34.27[a]	B3LYP/6-31+G(2d,p) // B3LYP/6-31G*	29.19
HF/6-31+G*	31.96[a]	MP2/6-31G**	33.22[b]
HF/6-311G**	35.47[a]	G2(MP2)	30.66[c]
B3LYP/6-31G*	34.96	CBS-Q	31.29[c]
B3LYP/6-31+G*	30.16		

[a] Scholz et al.[23] [b] Ball [24] [c] Without zero point energy correction. $\Delta ZPE = 2.5$ kcal/mol at the HF/6-31G* level of theory.

TABLE 4: Energetics for the Al_4O_6/H_2O System[a]

level of theory	molecular adsorption (kcal/mol)	transition sate[b] (kcal/mol)	dissociative adsorption (kcal/mol)
HF/6-31+G*	−39.29	−25.39	−59.45
B3LYP/6-311+G*//HF/6-31+G*	−38.98	−31.21	−56.14
MP2/6-311+G*//HF/6-31+G*	−44.56	−32.85	−59.32

[a] Energies are relative to the $Al_4O_6 + H_2O$ reactants at infinite separation and without zero point corrections. [b] Transition state for molecular to dissociative adsorption.

The model 2 barrier heights for the transition from molecular to dissociative adsorption are similar for the HF and MP2 calculations, 12 and 14 kcal/mol, respectively, while the B3LYP barrier is somewhat smaller at 8 kcal/mol. Dissociative adsorption is energetically preferred over molecular adsorption by 15 kcal/mol (MP2) to 20 kcal/mol (HF). Since this model is rather flexible, with the oxygen of the reactive site having only one neighboring aluminum below it (as opposed to two in the true crystal structure), it is possible that these values are an overestimation, since they may not represent all the steric strain for dissociative adsorption.

Parts b−d of Figure 5 show 1−2 dissociative adsorption of a single water molecule on the aluminum surface site of model 3a. For this pathway, dissociative adsorption counteracts 75−80% of the surface relaxation. As in model 2, moving from molecular to dissociative adsorption involves a shortening of the HF $Al_{surf}-O_{ads}$ distance to 1.72 Å and a simultaneous lengthening of one $Al_{surf}-O_{ads}$. Although the Al−O distances in model 3 are slightly longer, the 0.211 Å $Al_{surf}-O_{ads}$ decrease and the 0.410 Å $Al_{surf}-O_{ads}$ increase are almost identical to the changes found in model 2, also at the HF level. These changes occur to a smaller extent at the B3LYP level of theory with a respective 0.206 Å decrease and 0.310 Å increase in $Al_{surf}-O_{ads}$ and $Al_{surf}-O_{ads}$. At both levels of theory, the transition

TABLE 5: Energetics for 1−2 Dissociative Processes on Al_8O_{12}, Model 3a[a]

			dissociative adsorption			
	molecular adsorption				3 H_2O	
level of theory	1 H_2O	TS	1 H_2O	2 H_2O	$Al(OH)_3$	$Al(OH)_3H_2O$
HF/6-31+G* (3-21G)	−40.75	−24.62	−46.35	−98.71	−37.25	−58.78
HF/6-31+G*//HF/6-31+G*(3-21G)	−33.34	−15.93	−33.94	−93.53	−53.51	−75.04
B3LYP/6-31+G*//HF/6-31+G*(3-21G)	−31.84	−22.59	−32.78	−82.68	−47.50	−68.66
B3LYP/6-31+G*(3-21G)	−38.99	−30.81	−45.46			
B3LYP/6-31+G*//B3LYP/6-31+G*(3-21G)	−31.62	−22.34	−32.14			

[a] Energies (without ZPE) in kilocalories per mole, relative to the relaxed cluster and water molecule(s) at infinite separation.

state is midway between the structures for molecular and dissociative adsorptions. The distances between Al_{surf} and O atoms not directly involved in the reaction change by less than 1%. Distances between the oxygen to which the hydrogen adds and its neighboring second and third layer aluminum atoms increase by 2−3%. In general, the Al−O distances at the B3LYP/6-31+G*(3-21G) level of theory are 0.5−1.8% longer than at HF/6-31+G*(3-21G), with the exception of the Al_{surf}−O across which dissociation occurs, which is 3.8% shorter.

Energies for the TS and chemisorbed product of 1−2 dissociative adsorption on model 3a are given in Table 3. Molecular → dissociative adsorption is now exothermic by only 6 kcal/mol as compared to 15−20 kcal/mol for model 2. Such a decrease in the reaction exothermicity in proceeding from model 2 to model 3 is expected, since model 3 should better represent lattice strain effects. Furthermore, when the 6-31+G* basis set is used, molecular and dissociative adsorptions are essentially equal in energy.

HF and B3LYP values of the barrier height for the TS are 16−17 and 8−9 kcal/mol, respectively. The Hartree−Fock values are 2−3 kcal/mol larger than those for model 2, which can be attributed to the greater rigidity of model 3. Adsorption energetics determined at the B3LYP/6-31+G* level of theory on both the HF and B3LYP geometries are essentially identical.

Some possible products of multiple 1−2 dissociation events at a single aluminum surface site are shown in Figure 5e,f. For the model 3a calculations, two dissociations at the AlO_3 site display surprising behavior, in that two original Al−O interactions were broken and the aluminum atom subsequently moved to form a new interaction with a second nearest oxygen. As shown in Table 3, this causes a 50−60 kcal/mol lowering in energy, relative to single water dissociation. Complete removal of the surface aluminum atom to form $Al(OH)_3$ is higher in energy than double dissociation by 60 kcal/mol for the small basis set HF calculation and by 40 and 35 kcal/mol for the large basis set HF and B3LYP calculations. In all cases, further addition of a single molecularly adsorbed water to the $Al(OH)_3$ product decreases the energy by 21 kcal/mol. Furthermore, including two second shell water molecules to form $Al(OH)_3(H_2O)\cdot 2H_2O$ is predicted by Ruiz et al.[32] to stabilize the products by an additional 30 kcal/mol.

The 1−2 dissociation pathway was also examined at the HF/6-31+G*(3-21G) level of theory with model 3a embedded in a field of point charges. Results are summarized in Figure 6, where they are compared with the unembedded calculations. Including formal point charges without reoptimization stabilizes the TS and dissociative adsorption by 2 and 5 kcal/mol, respectively. The product of two dissociative adsorptions is also within 5 kcal/mol of the unembedded value. Reoptimization leads to an additional stabilization of 6 kcal/mol for the TS and 9 kcal/mol for the single dissociation. The changes with respect to the unembedded cluster are much smaller when the improved field of point charges is used. In single point

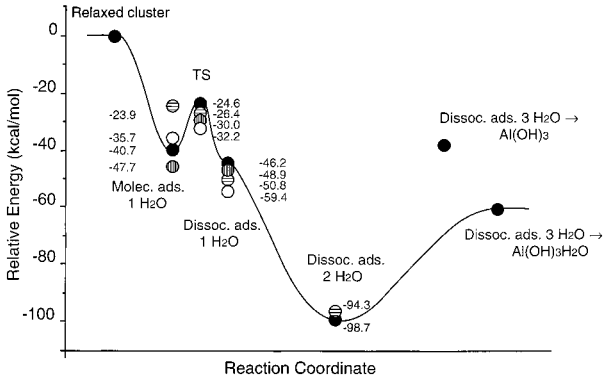

Figure 6. Adsorption energetics for the model 3 Al_8O_{12} structures of Figure 5, optimized at the HF/6-31+G*(3-21G) level of theory with and without embedding. Results are plotted relative to the reactants at infinite separation: ●, unembedded; ⊖, embedded single point calculation with bulk position formal point charges; ○, optimization in the previous embedding scheme. Improved embedded single point calcuations on $Al_{18}O_{27}$ are also shown as ⊕.

TABLE 6: Atomic Charge of the Surface Aluminum Atom[a]

	relaxed	molecular adsorption	dissociative adsorption
unembedded	2.30	2.21	2.27
embedded[b]	1.97	1.89	2.01
embedded[c]	1.91	1.84	1.95

[a] Determined by a natural population analysis[29] at the HF/6-31+G*(3-21G) level of theory. [b] Field of formal charges, unembedded geometry. [c] Field of formal charges, optimized geometry.

calculations the TS is stabilized by 3 kcal/mol, while dissociative adsorption is destabilized by 1 kcal/mol. The barrier of 16 kcal/mol is essentially the same as in the unembedded case. The barrier for dissociative adsorption for an $Al_{18}O_{27}$ cluster in this field is 18 kcal/mol.[31] Table 6 summarizes the Al_{surf} charges throughout the adsorption process. With the exception of the reacting surface oxygen, the charges on the remaining atoms do not change significantly over the course of the reaction.

In future work the long-range Coulomb interactions will be modeled more accurately with techniques such as the SCREEP method of Stefanovich and Truong[33] or the ONIOM method of Svensson et al.[34] However, the present results show that the effects of the Madelung field, while significant, are not overwhelming. Adsorption energies are qualitatively similar when a realistic field of point charges is included, while atomic charges, determined by natural population analysis,[29] are comparable for calculations done with and without the field (see Tables 2 and 6).

D. 1−4 Dissociative Adsorption. Model 3b was used to study 1−4 dissociative adsorption. Structures for the one water dissociation process appear in Figure 7b−d. Compared to the above 1−2 process, 1−4 dissociative adsorption has a slightly smaller effect on the aluminum position, with only 66−73%

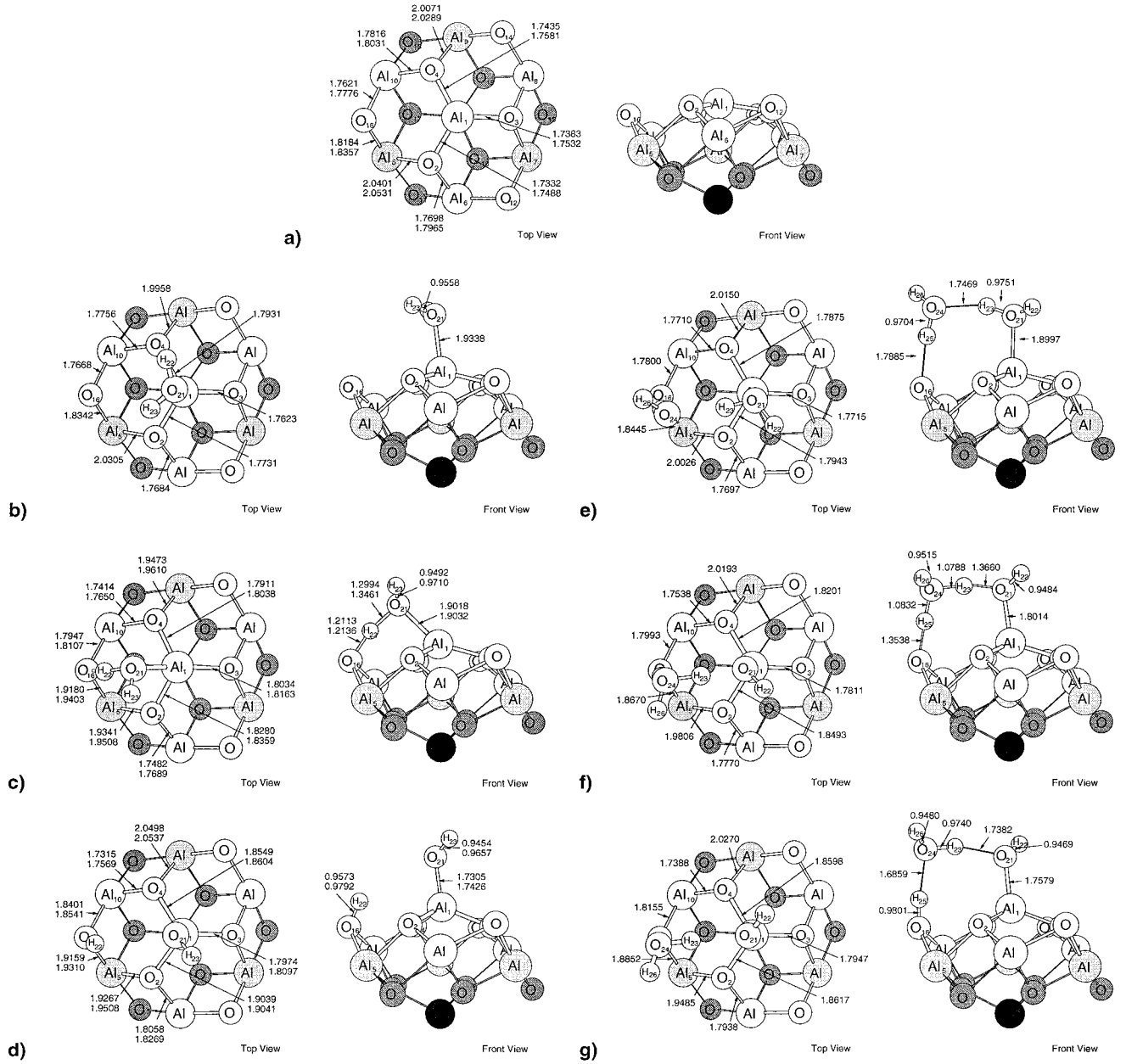

Figure 7. Model 3, set 2 at the HF/6-31+G*(3-21G) and (lower set of numbers) B3LYP/6-31+G*(3-21G) level of theory. The structures are as follows: (a) the Al_8O_{12} relaxed cluster, (b) molecular adsorption of one water molecule, (c) transition state for 1−4 dissociative adsorption, (d) 1−4 addition of water, (e) molecular adsorption of two water molecules, (f) transition state for 1−4 dissociative adsorption catalyzed by a second water molecule, and (g) 1−4 addition of water aided by a second water molecule.

TABLE 7: Energetics for 1−4 Dissociative Processes on Al_8O_{12}, Model 3b[a]

	one water process			two water process		
level of theory	molecular adsorption	TS	dissociative adsorption	molecular adsorption	TS	dissociative adsorption
HF/6-31+G* (3-21G)	−36.00	−13.23	−33.35	−58.36	−44.34	−55.82
HF/6-31+G*//HF/6-31+G* (3-21G)	−32.01	−8.67	−28.60			−50.05
B3LYP/6-31+G*//HF/6-31+G* (3-21G)	−31.07	−16.61	−27.25			−52.45
B3LYP/6-31+G* (3-21G)	−34.71	−20.14	−31.17			
B3LYP/6-31+G*//B3LYP/6-31+G* (3-21G)	−30.93	−16.11	−26.66			

[a] Energies (without ZPE) in kilocalories per mole, relative to the relaxed cluster and water molecule(s) at infinite separation.

recovery. Again, similar to the 1−2 dissociation, $Al_{surf}-O_{ads}$ decreases by roughly 0.2 Å at both HF and B3LYP levels of theory. However, the corresponding bond length increase is now spread over all three $Al_{surf}-O$ distances (2−7%) and the two $O_{16}-Al$ bonds (4%) to the second and third layers of aluminum atoms.

Model 3b energies for molecular and 1−4 dissociative adsorption of a single water molecule are given in Table 7. Comparing with the model 3a results in Table 5 shows that the energies for both molecular and dissociative adsorptions are higher for model 3b with the increase greater for dissociative adsorption. The resulting barrier to 1−4 dissociation is 5−7 kcal/mol higher than the 1−2 barrier, and, with the 6-31+G*

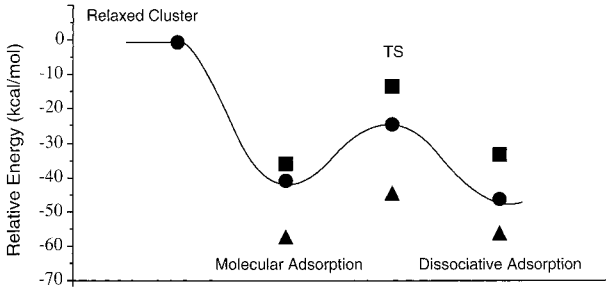

Figure 8. Comparison of the three types of dissociative adsorption of water at the HF/6-31+G*(3-21G) level of theory: ●, 1−2 addition, ■, single molecule 1−4 addition, and ▲, 1−4 addition catalyzed by a second water.

basis set, 1−2 dissociation of water is more exothermic than the 1−4 process by ca. 5 kcal/mol.

In molecular adsorption of two water molecules, Figure 7e, the first water is adsorbed to the aluminum site and the second is hydrogen bonded to both the first water and a surface oxygen. With two water molecules involved, the 1−4 dissociation (hydroxylation) process may be viewed in part as two O−H hydrogen bond/O−H bond exchanges. As shown in Figure 7f,g, the water adsorbed to the aluminum site transfers a hydrogen, H_{23}, to the second water, which in turn transfers its H_{25} atom to O_{16} of the surface. This type of hydroxylation causes a 0.14 Å decrease in $Al_{surf}-O_{ads}$. This change is ca. 0.06 Å smaller than those that occur in the single water processes. Furthermore, there is only a 60% reversal of the inward relaxation of the surface aluminum atom.

The difference between the molecular and 1−4 dissociative adsorption energies is small for both adsorption of one and two water molecules (see Table 7). The principal effect of the additional water molecule is to lower the barrier for 1−4 dissociative adsorption from 23 to 14 kcal/mol at the HF/6-31+G*(3-21G) level of theory. In comparison, the barrier for 1−2 adsorption is 16 kcal/mol. At the various levels of theory, 1−4 hydroxylation via the two water process is 21−25 kcal/mol more exothermic than the 1−4 single water process and 9−20 kcal/mol more exothermic than the 1−2 single water addition.

Energy profiles at the HF/6-31+G*(3-21G) level of theory for the three types of hydroxylation are compared in Figure 8. The energies of the hydroxylated products range from 30 to 55 kcal/mol. This is comparable to the 25 to 40 kcal/mol determined by Nelson et al.[35] from laser-induced thermal desorption and temperature programmed desorption experiments performed on a hydroxylated single-crystal α-Al_2O_3 (0001) surface and to the 37−41 kcal/mol average integral heat of chemisorption of water on nanocrystalline α-Al_2O_3 determined by McHale et al.[36] from high-temperature solution calorimetry.

E. Kinetics of Dissociative Adsorption. The above calculations show that both 1−2 and 1−4 H_2O dissociative adsorptions on α-Al_2O_3 proceed through a molecular adsorption intermediate, which is expected to attain thermal equilibrium with the bulk. Since the molecular adsorption step is barrierless, the rate of dissociative adsorption is determined by the molecular → dissociative adsorption step. The rate constants for both this and the reverse reaction were calculated from transition state theory (TST)[37] using the expression

$$k = (dk_B T/h) \exp(-\Delta G^{\ddagger}/RT) \quad (1)$$

where d is the reaction path degeneracy and $-\Delta G^{\ddagger}$ is the free energy difference between the transition state and reactants computed for the unembedded cluster at the HF/6-31+G*(3-21G) level of theory. The calculation was simplified by setting $d = 1$ and by assuming separable harmonic oscillations for all internal degrees of freedom for both the TS and the reactant using HF/6-31+G*(3-21G) vibrational frequencies scaled by 0.8973.[26]

For a more complete TST calculation, anharmonic effects should be included, particularly for the H_2O and OH torsions and for the low-frequency modes of the TS which are associated with the water molecule(s). It would also be necessary to use the actual value for d, which, however, is dependent upon the manner in which the internal modes are treated. For example, treating the H_2O torsion in the molecular adsorption state of Figure 4b as a rotor would contribute a factor of 3 to the reaction path degeneracy. Furthermore, for the transition state shown in Figure 4c, there is an enantiomeric TS where the H_{12} atom is on the opposite side of the $H_{13}-O_{11}-Al_1$ plane. This contributes an additional factor of 2, making $d = 6$. Similar effects are associated with the structures in Figures 5 and 7. In view of the above discussion, it was felt least ambiguous to use $d = 1$ for the work reported here. These calculated rate constants and A-factors may then be scaled by degeneracy factors which are most likely temperature dependent.[38]

Transition state theory rate constants and Arrhenius parameters at 300 and 1000 K are listed in Table 8 for the 1−2 and 1−4 dissociative adsorption processes studied here. For the 1−2 process, the rate constant of the forward reaction, molecular → dissociative adsorption, is considerably larger than that of the reverse reaction, while, for the 1−4 processes, the reverse rate constant is the larger. Particularly noteworthy is the speed

TABLE 8: Transition State Theory Rate Constants and Arrhenius Parameters for H_2O Dissociative Adsorption[a,b]

	300 K			1000 K		
model	k (s^{-1})	A	E_a (kcal/mol)	k (s^{-1})	A	E_a (kcal/mol)
1 H_2O, 1−2 dissociative on Al_4O_6						
forward→	1.1×10^{4}	1.5×10^{12}	11.18	5.8×10^{9}	2.0×10^{12}	11.59
←reverse	3.1×10^{-12}	9.8×10^{11}	32.25	7.2×10^{4}	7.4×10^{11}	32.08
1 H_2O, 1−2 dissociative on Al_8O_{12}						
→	1.1×10^{2}	8.1×10^{11}	13.52	9.6×10^{8}	1.1×10^{12}	13.92
←	4.0×10^{-3}	1.1×10^{12}	19.82	4.7×10^{7}	1.0×10^{12}	19.83
1 H_2O, 1−4 dissociative on Al_8O_{12}						
→	4.1×10^{-4}	2.4×10^{11}	20.27	8.4×10^{6}	2.5×10^{11}	20.47
←	3.4×10^{-2}	9.0×10^{11}	18.42	6.9×10^{7}	6.7×10^{11}	18.23
1 H_2O, 1−4 dissociative on Al_8O_{12}						
→	2.8×10^{4}	8.7×10^{11}	10.27	4.6×10^{9}	9.4×10^{11}	10.57
←	4.7×10^{5}	9.3×10^{11}	8.64	9.8×10^{9}	7.4×10^{11}	8.60

[a] Vibrational frequencies and zero point energies were computed at the HF/6-31+G*(3-21G) level of theory and were scaled by 0.8973. [b] The reaction path degeneracy was assumed to be 1.

TABLE 9: Stretching Frequencies of Molecularly Adsorbed Water[a]

type of water	symmetric stretch (cm^{-1})	antisymmetric stretch (cm^{-1})
H_2O	3653	3760
adsorbed on		
$Al(OH)_3$	3582	3673
model 2 (Figure 4b)	3566	3652
model 3a (Figure 5b)	3516	3633

[a] At the HF/6-31+G*(3-21G) level of theory, scaled by 0.8973.

TABLE 10: Surface O−H Stretching Frequencies[a]

type of O−H stretch		freq (cm^{-1})
Oxygen Bonded to a Single Al		
$Al(OH)_3$		3748, 3748, 3750
$Al(OH)_3 \cdot H_2O$		3745, 3753, 3769
model 2 (Figure 4d)	$O_{11}-H_{12}$	3747
model 3 (Figure 5d)	$O_{21}-H_{22}$	3729
(Figure 5e)	$O_{21}-H_{22}$	3719
	$O_{24}-H_{25}$	3748
Oxygen Bonded to Multiple Al		
model 2 (Figure 4d)	O_1-H_{13}	3671
model 3 (Figure 5d)	O_2-H_{23}	3560
(Figure 5e)	O_2-H_{23}	3685
	O_3-H_{26}	3529
(Figure 5f)		3710, 3710, 3716

[a] At the HF/6-31+G*(3-21G) level of theory, scaled by 0.8973.

of molecular → dissociative adsorption. The average lifetime for this step, i.e., *1/k*, is of the order of 10^{-2} s or less for both the single water 1−2 process and the two water 1−4 process. Furthermore, the barrier height obtained for the 1−2 addition with embedding and optimization in the sea of point charges indicates that hydroxylation may be as fast as 5 ps. *A*-factors for both the forward and reverse reactions are consistent with those for other H-atom transfers.[39]

F. O−H Stretching Frequencies. When water binds to a tricoordinate aluminum site, its overall vibrational structure is relatively undisturbed. At the HF/6-31+G* level of theory, the antisymmetric stretch of the "free" water molecule is 107 cm^{-1} larger than the symmetric mode. Table 9 shows that after adsorption, at the HF/6-31+G*(3-21G) level of theory, these modes are still clearly identifiable, with the separation between them changing by ±20 cm^{-1}. However, both modes are red-shifted by 70−140 wavenumbers. The size of this effect is correlated with the length of the O−H bonds. The largest shift occurs in model 3, where the average O−H bond is the longest (0.01 Å longer than in H_2O). For each of the models, the scaled bending frequency of water, 1612 cm^{-1}, increases by less than 10 wavenumbers upon adsorption.

The O−H stretching frequencies (scaled by 0.8973) of various hydroxyl groups are listed in Table 10. When the oxygen atom is bonded to two or three aluminum atoms, the frequencies fall in the relatively wide range of 3530−3720 cm^{-1}. In the cases where the OH group is bonded to a single aluminum, the stretching frequencies are higher and lie in a much smaller range of 3720−3770 cm^{-1}. The cluster that best represents the hydroxylated oxygen terminated surface (Figure 5f) has O−H frequencies of 3710−3716 cm^{-1} (after scaling). This shows good agreement with the 3720 cm^{-1} HREELS result of Coustet and Jupille.[2]

IV. Conclusions

The ab initio cluster calculations reported here yield surface relaxation parameters and energies for the aluminum terminated (0001) surface of α-aluminum oxide that are comparable to those determined from periodic ab initio methods[9,10] and experiment.[4,5] The calculated energies for water adsorption also compare well to the experimental values of 25−41 kcal/mol.[35,36] Calculations on unembedded and embedded clusters indicate that the exothermicities of molecular and dissociative adsorption of water are roughly the same. Of the three processes examined in this paper, a single hydroxylation event at an aluminum site proceeds most favorably by either 1−4 addition catalyzed by a second water molecule or by direct 1−2 addition. Transition state theory calculations indicate that hydroxylation of the surface is rapid, occurring within 10^{-2} s after H_2O has molecularly adsorbed, although a preliminary inclusion of the Madelung field indicates that this may be as fast as 5 ps. Investigation of multiple 1−2 dissociation events at a single surface site indicate that the surface aluminum may undergo limited motion along the surface to interact with a previously second nearest neighbor oxygen atom. Furthermore, under appropriate circumstances, removal of surface aluminum atoms to form a hydroxylated oxygen terminated surface is possible. In the presence of excess quantities of water, it is likely that all the interactions examined in this paper, as well as a variety of other processes, occur to some extent.

Acknowledgment. Special thanks to William F. Schneider and Kenneth C. Hass of the Ford Motor Co. for communicating the results of their Car−Parrinello calculation and for the many helpful and thought provoking conversations. Thanks also to C&IT at Wayne State University for generous amounts of computing time. This work was supported by the Office of Naval Research Grant N00014-96-1-1079.

References and Notes

(1) Gautier, M.; Renaud, G.; Van, L. P.; Villette, B.; Pollak, M.; Thromat, N.; Jollet, F.; Duraud, J.-P. *J. Am. Ceram. Soc.* **1994**, *77*, 323.
(2) Coustet, V.; Jupille, J. *Surf. Interface Anal.* **1994**, *22*, 280. Coustet, V.; Jupille, J. *Surf. Sci.* **1994**, *307*−*309*, 1161.
(3) Stará, I.; Zeze, D.; Matolín, V.; Pavluch, J.; Gruzza, B. *Appl. Surf. Sci.* **1997**, *115*, 46.
(4) Guenard, P.; Renaud, G.; Barbier, A.; Gautier-Soyer, M. *Mater. Res. Soc. Symp. Proc.* **1996**, *437*, 15. Guenard, P. Ph.D. Thesis, l'Universite Joseph Fourier−Grenoble I, 1996.
(5) Ahn, J.; Rabalais, J. W. *Surf. Sci.* **1997**, *388*, 121.
(6) Tasker, P. W. *Adv. Ceram.* **1988**, *10*, 176.
(7) Mackrodt, W. C. *J. Chem. Soc., Faraday Trans. 2* **1989**, *85*, 541. Mackrodt, W. C. *Philos. Trans. R. Soc. London A* **1992**, *341*, 301.
(8) Guo, J.; Ellis, D. E.; Lam, D. J. *Phys. Rev. B* **1992**, *45*, 13647.
(9) Pisani, C.; Causà, M.; Dovesi, R.; Roetti, C. *Prog. Surf. Sci.* **1987**, *25*, 119. Causà, M.; Dovesi, R.; Pisani, C.; Roetti, C. *Surf. Sci.* **1989**, *215*, 259. Salasco, L.; Dovesi, R.; Orlando, R.; Causà, M.; Saunders: V. R. *Mol. Phys.* **1991**, *72*, 267.
(10) Manassidis, I.; De Vita, A.; Gillan, M. J. *Surf. Sci. Lett.* **1993**, *285*, L517. Manassidis, I.; Gillan, M. J. *J. Am. Ceram. Soc.* **1994**, *77*, 335.
(11) Puchin, V. E.; Gale, J. D.; Schluger, A. L.; Kotomin, E. A.; Günster, J.; Brause, M.; Kempter, V. *Surf. Sci.* **1997**, *370*, 190.
(12) Nygren, M. A.; Gay, D. H.; Catlow, C. R. A. *Surf. Sci.* **1997**, *380*, 113.
(13) Kinloch, A. J. *Adhesion and Adhesives: Science and Technology*; Chapman and Hall: London, 1987.
(14) Lee, L. H., Ed. *Fundamentals of Adhesion*; Plenum: New York, 1991.
(15) Debski, M.; Shanahan M. E. R.; Schultz, J. *Int. J. Adhes. Adhes.* **1986**, *6*, 145.
(16) Hong, S. G.; Boerio, F. J. *J. Adhes.* **1995**, *49*, 133.
(17) *Cerius*[2]; BIOSYM/Molecular Simulations: San Diego, CA, 1995.
(18) Taken from the crystal database of Cerius[2] [17] with lattice parameters of $a = 4.748$, $c = 12.954$, and Al−O distances of 1.8524 and 1.9628 Å.
(19) Frisch, M. J.; Trucks, G. W.; Schlegel, H. B.; Gill, P. M. W.; Johnson, B. G.; Robb, M. A.; Cheeseman, J. R.; Keith, T.; Petersson, G. A.; Montgomery, J. A.; Raghavachari, K.; Al-Laham, M. A.; Zakrzewski, V. G.; Ortiz, J. V.; Foresman, J. B.; Cioslowski, J.; Stefanov, B. B.; Nanayakkara, A.; Challacombe, M.; Peng, C. Y.; Ayala, P. Y.; Chen, W.; Wong, M. W.; Andres, J. L.; Replogle, E. S.; Gomperts, R.; Martin, R. L.; Fox, D. J.; Binkley, J. S.; Defrees, D. J.; Baker, J.; Stewart, J. P.; Head-

Gordon, M.; Gonzalez, C.; Pople, J. A. *GAUSSIAN 94, Revision C.3*; Gaussian, Inc.: Pittsburgh, PA, 1995.

(20) Becke, A. D. *J. Chem. Phys.* **1993**, *98*, 5648.

(21) Curtiss, L. A.; Raghavachari, K.; Pople, J. A. *J. Chem. Phys.* **1993**, *98*, 1293L.

(22) Petersson, G. A.; Tensfeldt, T. G.; Montgomery, J. A., Jr. *J. Chem. Phys.* **1991**, *94*, 6091.

(23) Scholz, G.; Stösser, R.; Bartoll, J. *J. Phys. Chem.* **1996**, *100*, 6518.

(24) Ball, D. W. *J. Phys. Chem.* **1995**, *99*, 12786.

(25) Hass, K. C.; Schneider, W. F.; Curioni, A.; Andreoni, W. Unpublished work.

(26) Krossner, M.; Scholz, G.; Stösser, R. *J. Phys. Chem. A* **1997**, *101*, 1555.

(27) Since only some of the surface oxygen atoms are optimized, we chose to use the surface area of the unrelaxed unit cell, as described in the Introduction, rather than use the surface area of the cluster.

(28) Puchin et al. predict a 2−4 times larger surface relaxation energy of 6.23 eV/unit cell or 5.09 J/m^2.

(29) Glendenning, E. D.; Reed, A. E.; Carpenter, J. E.; Weinhold, F. *NBO*, Version 3.1; University of Wisconsin: Madison, 1990.

(30) Ching, Y. W.; Xu, Y. N. *J. Am. Ceram. Soc.* **1994**, *77*, 404.

(31) $Al_{18}O_{27}$ is the next largest cluster after Al_8O_{12} that maintains reasonable bonding, appropriate stoichiometry, and correct symmetry. The $Al_{18}O_{27}$ cluster was formed by adding Al and O atoms to the unembedded relaxed Al_8O_{12} cluster. These atoms were represented by the 3-21G basis set and were placed in bulk positions with the surface aluminums relaxed in accord with the Al_8O_{12} model.

(32) Ruiz, J. M.; McAdon, M. H.; Garcés, J. M. *Phys. Chem. B* **1997**, *101*, 1733.

(33) Stefanovich, E. V.; Truong, T. N. *J. Phys. Chem. B* **1998**, *102*, 3018.

(34) Svensson, M.; Humbel, S.; Froese, R. D. J.; Matsubara, T.; Sieber, S.; Morokuma, K. *J. Phys. Chem.* **1996**, *100*, 19357.

(35) Nelson, C. E.; Elam, J. W.; Cameron, M. A.; Tolbert, M. A.; George, S. M. *Surf. Sci.*, submitted for publication.

(36) McHale, J. M.; Auroux, A.; Perrotta, A. J.; Navrotsky, A. *Science* **1997**, *277*, 788.

(37) Glasstone, S.; Laidler, K. J.; Eyring, H. *The Theory of Rate Processes*, McGraw-Hill Book Co., Inc.: New York, 1941.

(38) Peslherbe, G. H.; Hase, W. L. *J. Chem. Phys.* **1996**, *105*, 7432.

(39) Robinson, P. J.; Holbrook, K. A. *Unimolecular Reactions*; John Wiley and Sons: New York, 1972; p 209.